Numerical prediction of absolute crystallization rates in hard-sphere colloids

S. Auer[a] and D. Frenkel
FOM Institute for Atomic and Molecular Physics, Kruislaan 407, 1098 SJ Amsterdam, The Netherlands

(Received 8 September 2003; accepted 11 November 2003)

Special computational techniques are required to compute absolute crystal nucleation rates of colloidal suspensions. Using crystal nucleation of hard-sphere colloids as an example, we describe in some detail the novel computational tools that are needed to perform such calculations. In particular, we focus on the definition of appropriate order parameters that distinguish liquid from crystal, and on techniques to compute the kinetic prefactor that enters in the expression for the nucleation rate. In addition, we discuss the relation between simulation results and theoretical predictions based on classical nucleation theory. © *2004 American Institute of Physics.*
[DOI: 10.1063/1.1638740]

I. INTRODUCTION

A collection of identical hard spheres is probably the simplest model system that undergoes a first order freezing transition. For low packing fractions the particles are in a liquid state, but when the packing fraction exceeds a value of 49.4% an ordered solid state becomes more stable. This was first shown in computer simulations by Hoover and Ree[1] in 1968. Initially, liquids and solids of hard spheres were purely theoretical concepts, but in the 1970s and 1980s experimental realizations of the hard sphere were developed, viz. suspensions of hard, uncharged colloids.[2,3] For instance, in 1986, Pusey and van Megen showed that polymethylmethacrylate (PMMA) particles stabilized by chemically grafted polyhydroxystearic acid (PHSA) reproduced closely the equilibrium phase behavior expected of hard spheres.[3] Nowadays other realizations are also known.[4,5]

Whereas initially the experimental study of hard-sphere colloids focused on the equilibrium phase behavior, during the past decade the focus has shifted towards the experimental study of the phase transition kinetics of hard-sphere colloids.[6–8] Crystallization in colloidal suspensions is interesting because it can be studied in considerable detail. The major problem of experimental investigations of crystallization kinetics in atomic systems is the high speed of nucleus formation and subsequent crystal growth, as well as the difficulty of preventing heterogeneous nucleation. Colloidal particles are much larger than atoms and therefore crystallize on a time scale that is about ten orders of magnitude longer than that in atomic systems. Moreover, because of their size, colloids can be probed by powerful optical methods such as time-resolved static laser light scattering and confocal microscopy. In these systems it is also somewhat easier to control heterogeneous nucleation. In a recent letter[9] we reported a numerical study of the crystallization kinetics in hard-sphere colloids. This work demonstrated that it is now possible to make parameter-free predictions of crystal nucleation rates that could be compared quantitatively with experiment. Interestingly, there are some significant differences between the numerical predictions and the experimental results. This is surprising as so far experiments and computer simulations of hard spheres agree on almost every physical property (for an overview see, e.g., Ref. 10).

In the present paper we give a detailed description of the numerical techniques that are needed to predict colloidal crystal nucleation rates. We then proceed to discuss our numerical results in more detail than was possible in Ref. 9. The rest of this paper is organized as follows: First, in Sec. II, we briefly review classical nucleation theory (CNT) and show how it is used for the interpretation of the experimental data. Next, in Sec. III, we give a detailed description of the numerical techniques needed for the calculation of a nucleation rate. In Sec. III A we discuss the calculation of the nucleation barrier and, in Sec. III B, of the kinetic prefactor. The structure of the crystal nuclei is discussed in Sec. IV.

II. CNT AND NUCLEATION RATE EXPERIMENTS

The main problem when studying crystal nucleation, experimentally as well as in computer simulations, is that crystal nucleation is an activated process. First, small crystal nuclei need to form spontaneously in a supersaturated solution, but unless their size exceeds a critical value, they will redissolve rather than grow. According to CNT the free energy of a spherical nucleus that forms in a supersaturated solution contains two terms. The first is a bulk term, which takes care of the fact that the solid phase is more stable than the liquid. This term is negative and proportional to the volume of the nucleus. The second term is the surface term which describes the free energy needed to create a liquid–solid interface. This term is positive and proportional to the surface area of the nucleus. The (Gibbs) free energy of a spherical nucleus of radius R has the following form:

$$\Delta G = \tfrac{4}{3}\pi R^3 \rho_s \Delta\mu + 4\pi R^2 \gamma, \tag{1}$$

where ρ_s is the number density of the bulk solid, $\Delta\mu$ the difference in chemical potential between the liquid and the

[a]Present address: Department of Chemistry, Cambridge University, Lensfield Road, Cambridge, CB2 1EW, UK.

solid, and γ is the liquid–solid surface free energy density. The function ΔG has a maximum at $R=2\gamma/(\rho_s|\Delta\mu|)$ and the corresponding height of the nucleation barrier is given by

$$\Delta G_{\rm crit}=\frac{16\pi}{3}\frac{\gamma^3}{(\rho_s|\Delta\mu|)^2}. \tag{2}$$

For small nuclei the surface term dominates and the free energy increases. Only if this nucleus exceeds a critical size does its free energy decrease and the liquid start to crystallize. The probability for the formation of a critical nucleus depends exponentially on its free energy of formation,

$$P_{\rm crit}\propto\exp(-\Delta G_{\rm crit}/k_BT), \tag{3}$$

and the crystal nucleation rate is given by the product of $P_{\rm crit}$ and a kinetic factor κ, which describes the rate with which a critical nucleus grows. The corresponding expression for the nucleation rate from CNT is given by

$$I=\kappa\exp\left[-\frac{16\pi}{3k_BT}\frac{\gamma^3}{(\rho_s|\Delta\mu|)^2}\right], \tag{4}$$

where

$$\kappa=24\rho_l Z D_S n_{\rm crit}^{2/3}/\lambda^2. \tag{5}$$

Here ρ_l is the number density of the liquid, $Z=\sqrt{|\Delta\mu|/6\pi k_BTn_{\rm crit}}$ is the Zeldovich factor, D_S is a self-diffusion coefficient, $n_{\rm crit}$ is the number of particles in the critical nucleus, and λ is a typical diffusion distance for particles to attach to the critical nucleus. The above expression for the nucleation rate is the one most commonly used to analyze crystal nucleation rate experiments. The problem with the CNT approach is however that, in most cases, neither λ nor γ are accurately known. Both parameters are used to fit the experimental observations. The result is often that estimates for the kinetic prefactor seem unphysical. To illustrate the problems that can arise from this approach we give an example from recent experiments on crystallization in hard-sphere colloids. In Fig. 1 we show the results from crystallization rate measurements in hard-sphere colloids, performed by two different groups.[7,11] For this system the difference in chemical potential between the two phases can be calculated accurately from existing analytical expressions for the equation of state. The curves in the figure result from a two parameter fit of Eq. (4) to the experimental data. Palberg[12] fitted the data from Harland and van Megen[7] and obtained $\gamma=0.5k_BT/\sigma^2$ and $\lambda=17d_{\rm NN}$, while for the data from Heymann *et al.*[11] he found $\gamma=0.54k_BT/\sigma^2$ and $\lambda=2.8d_{\rm NN}$, where σ is the particle diameter and $d_{\rm NN}$ is the nearest neighbor distance. The functional form is described well by the CNT expression for the nucleation rate, but the estimates for the surface free energy are now known to be rather low.[13] In addition, the values of the effective jump length λ seem rather large. However, as the experimental results could be fitted with Eq. (4), there was little reason to doubt the values of the fit parameters thus obtained from experiment. As the crystal nucleation rate is a difficult quantity to measure there is a clear need for a first principle prediction of a crystal nucleation rate.

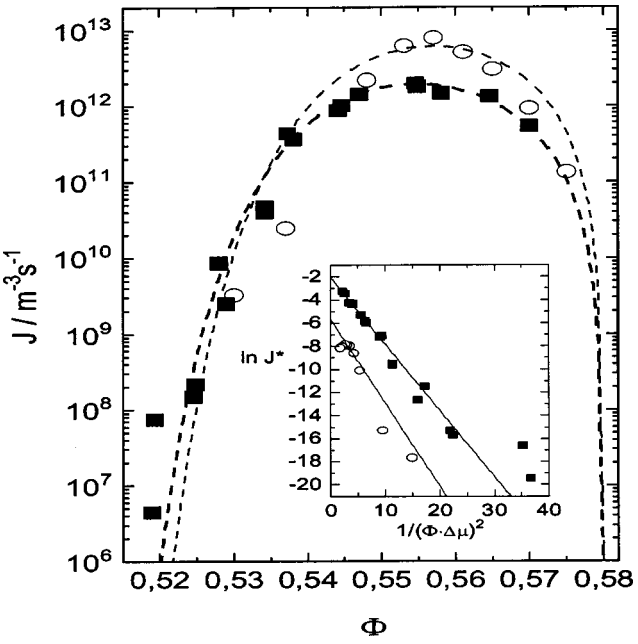

FIG. 1. Measured crystal nucleation rates I as of function of volume fraction ϕ in a system of hard-sphere colloids. The data are taken from Ref. 7 (open circles) and Ref. 11 (filled cubes). The lines result from a two parameter fit of Eq. (4) to the experimental data. The inset shows the dimensionless nucleation rate densities plotted logarithmically vs $1/(\phi\Delta\mu)^2$. The figure is taken from Ref. 12.

In this paper we approach this problem by using a combination of numerical techniques to simulate the crystal nucleation process. We use umbrella sampling, in combination with a local bond-order analysis for the identification of crystal nuclei, to compute the shape and the height of the nucleation barrier and to study the structure of critical nuclei. In addition we perform kinetic Monte Carlo simulations to compute the kinetic prefactor. The resulting nucleation rate can be compared directly with experiments without any adjustable parameter. The numerical techniques are described in the following.

III. NUMERICAL METHOD

Simulating the crystallization process is a computational challenge, precisely because crystal nucleation is an activated process. This implies that the formation of small crystal nuclei in a supersaturated liquid is infrequent but, when it happens, the process is quite fast, i.e., it proceeds on a time scale that can be followed in a molecular simulation. For instance, experimentally measured nucleation rates are typically on the order of $\mathcal{O}(10^1)$ to $\mathcal{O}(10^6)$ nuclei per $\rm cm^3$ per s. We can estimate the number of time steps needed in a molecular dynamics (MD) simulation to observe one nucleation event. In a large-scale computer simulation, it is feasible to study the dynamics of $\mathcal{O}(10^6)$ particles, but the number of particles in a typical simulation is some two to three orders of magnitude less. For an atomic liquid, the volume of a simulation box containing one-million particles is of order $\mathcal{O}(10^{-15})$ $\rm cm^3$. If one-million nuclei form per second in 1 cubic centimeter, then it will take, on average, 10^9 seconds for a nucleus to form in a system of one-million particles. As

the typical time step in a molecular simulation (MD) is on the order of femtoseconds, this implies that it would take some 10^{24} MD time steps to observe a single nucleation event under experimental conditions.

This example illustrates why it will be difficult to compute nucleation rates using conventional MD simulations. One way around this problem is to simulate a system at a much higher supersaturation, where the free-energy barrier for the formation of crystal nuclei is sufficiently low to allow the system to crystallize spontaneously on a time scale that is accessible in a MD simulation. The problem with this approach is that, at such extreme supersaturations, crystallization may proceed differently than at moderate supersaturations. For example, at high supersaturations, many crystal nuclei may form simultaneously and may interact in an early stage of their development. It then becomes difficult to compare the computed crystallization rates with predictions based on CNT.

In order to study crystal nucleation at moderate supersaturation, we exploit the fact that the crystallization rate is determined by the product of a static term, namely the probability for the formation of a critical nucleus P_{crit}, and a kinetic factor κ that describes the rate at which such nuclei grow. We use umbrella sampling to compute P_{crit} and kinetic Monte Carlo simulations to compute κ. The computed nucleation rates can be directly compared to experimental data.

In the following we first discuss the calculation of the cluster size distribution, after that we turn to the calculation of the kinetic prefactor.

A. Calculation of the cluster size distribution

The probability to form a crystal nucleus of size n can be approximated by $P(n)=N_n/N$, where N_n is the number of crystal nuclei of size n in a system containing N particles,[14,15] see also Appendix A. The approximation becomes better as N_n/N becomes smaller, i.e., when the spontaneous formation of clusters is rare. Knowledge of the ratio N_n/N allows us to define the Gibbs free energy $\Delta G(n)$ for the formation of a nucleus of size n,

$$\frac{N_n}{N}=\exp[-\Delta G(n)/k_BT]. \tag{6}$$

Before we can calculate N_n in a Monte Carlo simulation we need to have a numerical technique that enables us to distinguish between particles in a liquid and solid environment. To this end, we use a local bond-order analysis which is described below.

1. Identification of solid cluster: Local bond-order analysis

The local bond-order analysis we use was introduced by Steinhardt *et al.*[16] and applied to study nucleation by Frenkel and co-workers.[17–19] The advantage of this analysis is that it is only sensitive to the overall degree of crystallinity in the system, but independent of any specific crystal structure. This requirement is important as otherwise we might force the system to crystallize in a specific structure. A practical advantage is that these bond-order parameters are rotationally invariant and that therefore the identification of crystallites does not depend on their orientation in space.

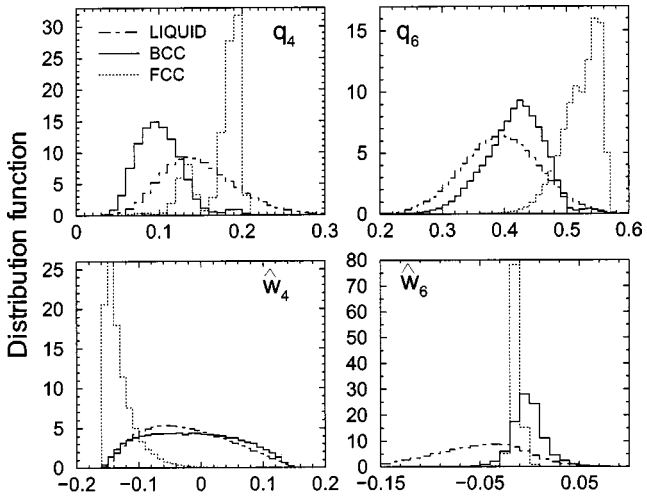

FIG. 2. Distribution functions of the local bond-order parameters: q_4, q_6, $\hat{w}_4$, and $\hat{w}_6$ from Monte Carlo simulations in a hard-sphere system. Here the cutoff radius r_q for the local environment of a particle is chosen to be 1.4σ, where σ is the hard-core diameter. This means that we included the first, and in some cases also the second, nearest neighbors.

The local bond-order parameters are a measure of the local structure around a particle and are constructed as follows. First we define a $(2l+1)$ dimensional complex vector with the components

$$q_{lm}(i)=\frac{1}{N_b(i)}\sum_{j=1}^{N_b(i)} Y_{lm}(\hat{\mathbf{r}}_{ij}),$$

where the sum goes over all neighboring particles $N_b(i)$ of particle i. Neighbors are usually defined as all particles that are within a given radius r_q around a particle. $Y_{lm}(\hat{\mathbf{r}}_{ij})$ are the spherical harmonics evaluated for the normalized direction vector $\hat{\mathbf{r}}_{ij}$ between the neighbors. The orientation of the unit vector $\hat{\mathbf{r}}_{ij}$ is determined by the polar and azimuthal angles θ_{ij} and ϕ_{ij}. The rotationally invariant local bond-order parameters are then defined as follows:

$$q_l(i)=\left(\frac{4\pi}{2l+1}\sum_{m=-l}^{l}|q_{lm}(i)|^2\right)^{1/2}$$

and

$$\hat{w}_l(i)=\frac{w_l(i)}{(\Sigma_{m=-l}^{l}|q_{lm}(i)|^2)^{3/2}}$$

with

$$w_l(i)=\sum_{\substack{m_1,m_2,m_3\\ m_1+m_2+m_3=0}}\begin{pmatrix} l & l & l\\ m_1 & m_2 & m_3\end{pmatrix} q_{lm_1}(i)q_{lm_2}(i)q_{lm_3}(i).$$

The term in large parentheses in the last equation is the Wigner-3j symbol. In Fig. 2 we show typical distribution functions of the local bond-order parameters q_4, q_6, $\hat{w}_4$, $\hat{w}_6$ calculated in a Monte Carlo simulation of hard spheres under conditions close to the coexistence point, where the liquid and the solid phase are equally stable. The figure illustrates that there is some separation between the distribution func-

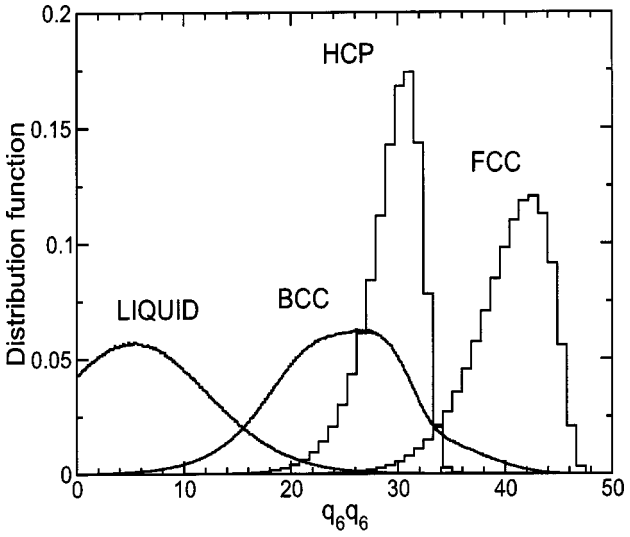

FIG. 3. Distribution functions of the dot product $\mathbf{q}_6(i)\cdot\mathbf{q}_6(j)$ from Monte Carlo simulations in a hard-sphere system.

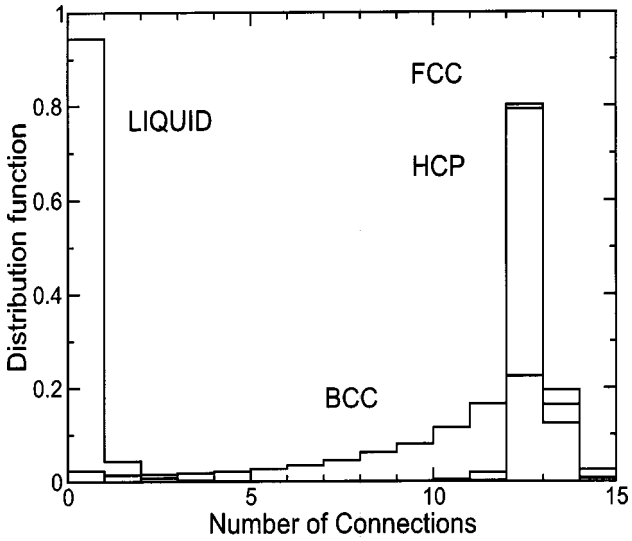

FIG. 4. Distribution functions of the number of connections per particle from Monte Carlo simulations in a hard-sphere system.

tions obtained from the liquid and those obtained from the solid. Sometimes, there is even a separation between the solid structures themselves, a property that we will use later to distinguish between different solid structures. For the identification of solidlike particles we have to choose an order parameter that is able to distinguish between the liquid on the one hand, and all possible solid structures, on the other. From Fig. 2 we see that q_6 has some of the desired properties, as the values of the solid phases are all shifted to higher values compared to the liquid. These order parameters are sensitive to the degree of orientational correlations of the vectors that join neighboring particles. In simple liquids we expect that there are no preferred orientations around a particle and therefore the correlations decay rapidly. In contrast, for a particle with a solidlike environment the vectors are correlated and as a result there should be a clear separation between distribution functions for the bond-order parameter. For this reason we can enhance the selectivity of the method by calculating the correlation function of the vectors $\mathbf{q}_6$ of neighboring particles i and j,

$$\mathbf{q}_6(i)\cdot\mathbf{q}_6(j)=\sum_{m=-6}^{6} q_{6m}(i)\cdot q_{6m}^{*}(j),$$

where the $*$ indicates the complex conjugate. In Fig. 3 we show the corresponding distribution functions for a hard-sphere system. Note that we did not attempt to normalize the dot-product. The relevant solid structures, which for the hard-sphere system are fcc, hcp, and bcc, yield much higher values for the dot-product than the liquid. We now define two neighboring particles i and j to be connected, if the dot-product described above exceeds a certain threshold. In the case of hard spheres this threshold is set to 20. By using this definition we can correctly identify effectively all particles in a solid to be solidlike, however also in the liquid it happens quite frequently that a particle has more than one connection. To illustrate this, we show in Fig. 4 the distribution functions for the number of connections per particle. Note, that the peak for the solid structures is at 12 for fcc, hcp, and around 13 for bcc. These numbers correspond to the first, or first and second nearest neighbors, which were included in the local environment. For the bcc structure the peak is slightly shifted to lower values, which is due to the fact that the bcc structure is relatively disordered. The bcc lattice of monodisperse hard-spheres melts spontaneously. We found, however, that a slightly polydisperse (3%) bcc crystal is mechanically stable. We used such a crystal to study the bcc bond-order properties. Thus far, we have no clear separation between solidlike and liquidlike particles, because the order-parameter distributions overlap. We therefore apply a more stringent criterion to distinguish between solid and liquid. To this end, we impose a threshold on the number of connections a particle has with its neighbors. All particles with less connections than this threshold are considered to be liquidlike. We should bear in mind that, in a small nucleus, most particles are at the surface. These should be recognized as solidlike. We found this is achieved if we choose threshold value between 6 and 8. The present analysis provides us with an unambiguous local criterion to identify solidlike particles. Finally, we need a criterion to identify which solid particles belong to a single cluster. For this purpose, we used a simple distance criterion: if two solidlike particles are closer than a certain threshold distance, then they belong to the same cluster. The values that we choose for this were between 1.5σ and 2σ.

2. Monte Carlo simulation

To calculate the nucleation barrier, we need to sample the equilibrium distribution function for the probability $P(n)$, see Eq. (6). In Appendix A we derived this probability to be approximately N_n/N, where N_n is the number of clusters of size n in a system containing N particles, see Eq. (A5). In the preceding section we illustrated how a local bond-order analysis can be used to identify clusters in a system. We now use these techniques to compute the cluster-size distribution by Monte Carlo simulation.

In all cases we performed Monte Carlo simulations in the isobaric–isothermal (NPT) ensemble. In this ensemble the average of a microscopic quantity A is given by

$$\langle A\rangle_{NPT}=\frac{\int dV\int d\mathbf{r}^N A(\mathbf{r}^N)\exp[-\beta(U(\mathbf{r}^N)+PV)]}{\int dV\int d\mathbf{r}^N \exp[-\beta(U(\mathbf{r}^N)+PV)]},$$

where $U(\mathbf{r}^N)$ is the potential energy of the system with particle positions $\mathbf{r}^N$. $\beta=1/(k_BT)$ is the reciprocal of the thermal energy, N the number of particles, and P the applied pressure. In a Metropolis Monte Carlo simulation the above ensemble average is approximated by

$$\langle A\rangle_{NPT}\approx\frac{1}{M}\sum_{i=1}^{M} A(\mathbf{r}_i^N), \tag{7}$$

where M is the total number of measurements and $A(\mathbf{r}_i^N)$ the value of our property A associated with configuration $\mathbf{r}_i^N$.

In the case of crystal nucleation we need to calculate the average number of clusters of size n and Eq. (7) becomes

$$\langle N_n\rangle_{NPT}\approx\frac{1}{M}\sum_{i=1}^{M} N_n(\mathbf{r}_i^N).$$

As an example we show the result from a Monte Carlo simulation in a system of hard spheres. In the simulation we used $N=3375$ particles and applied a pressure $\beta P\sigma^3=16$. At this pressure, the liquid phase is metastable with respect to the solid, but does not crystallize spontaneously as the Gibbs free-energy barrier between the two states is too high. The temperature T does not play a role in that system. After equilibrating the system, one could in principle measure the cluster size distribution after every Monte Carlo move, however this would be computationally expensive and statistics would still be poor, as the measurements are strongly correlated. Instead we measure the cluster size distribution after one trajectory, which consists of 20 moves per particle plus about ten volume moves. The total length of the simulation was 100 000 trajectories. In this simulation we could measure the probability distribution $P(n)$ up to cluster sizes of $n=15$ particles. The corresponding Gibbs free energy for the formation of such a cluster is shown in Fig. 6. The formation of larger cluster was so rare that the statistical accuracy was too poor. In order to sample larger cluster sizes we needed to apply the umbrella sampling technique of Torrie and Valleau,[20] which we describe in turn.

3. Umbrella sampling with parallel tempering

The umbrella sampling scheme was proposed to handle situations where important contributions to the ensemble average come from configurations whose Boltzmann factor is small, leading to poor statistical accuracy. The method is based on the idea that the ensemble average can be rewritten as follows:

$$\begin{aligned}\langle A\rangle_{NPT}&=\frac{\int dV\int d\mathbf{r}^N A(\mathbf{r}^N)\exp[-\beta(U(\mathbf{r}^N)+PV)]W^{-1}W}{\int dV\int d\mathbf{r}^N \exp[-\beta(U(\mathbf{r}^N)+PV)]W(\mathbf{r}^N)^{-1}W(\mathbf{r}^N)}\\&\quad\times\frac{\int dV\int d\mathbf{r}^N W(\mathbf{r}^N)\exp[-\beta(U(\mathbf{r}^N)+PV)]}{\int dV\int d\mathbf{r}^N W(\mathbf{r}^N)\exp[-\beta(U(\mathbf{r}^N)+PV)]}\\&=\frac{\langle A/W(\mathbf{r}^N)\rangle_W}{\langle W(\mathbf{r}^N)^{-1}\rangle_W},\end{aligned} \tag{8}$$

where we have introduced a, as yet, unspecified weighting function $W(\mathbf{r}^N)=\exp[-\beta\omega(\mathbf{r}^N)]$, where $\omega(\mathbf{r}^N)$ is the so-called biasing potential. Instead of performing a Monte Carlo simulation using the original Boltzmann distribution function, we now sample phase space according to the biased distribution function $\exp[-\beta U(\mathbf{r}^N)+PV)]W(\mathbf{r}^N)$, which is indicated by the subscript $\langle\cdots\rangle_W$. By specifying the weighting function W we can force the system to sample in that region of phase space which is important to improve the statistical accuracy.

In the case of crystal nucleation we can calculate the ensemble average according to the weighted ensemble, Eq. (8), as follows:

$$\langle N_n\rangle_{NPT}\approx\frac{\Sigma_i^M[N_n(\mathbf{r}_i^N)/W(\mathbf{r}_i^N)]}{\Sigma_i^M[W(\mathbf{r}_i^N)^{-1}]},$$

where the sum goes over all measurements M. We now need to consider the choice of the weighting function.

In Appendix A we showed that the probability for the formation of a larger cluster is so small, it can be approximated by the probability to find one cluster of a certain size in the system, see Eq. (A3). For this reason we can choose a bias potential that just controls the size of the largest cluster in the system. In all cases the bias potential was chosen to be a harmonic function of the size of the largest cluster in the system

$$\omega[n(\mathbf{r}^N)]=\tfrac{1}{2}k_n[n(\mathbf{r}^N)-n_0]^2.$$

The constant k_n determines the range of sizes sampled in one simulation, whereas the minimum n_0 determines which cluster sizes are sampled most.

The implementation of the biasing potential in the Monte Carlo simulation is straightforward. As in the unbiased run we try to avoid calculating the size of the largest cluster after every Monte Carlo move. Instead we perform a trajectory of a certain number of Monte Carlo moves per particle according to the unbiased potential $U(\mathbf{r}^N)$. We then recalculate the cluster size and accept or reject the whole trajectory according to the pure biasing potential $\exp[-\beta\Delta\omega]$, where $\Delta\omega$ is the difference in the biasing potential after and before the trajectory. This is equivalent to applying the bias potential after every trial move, but computationally much cheaper.

Intuitively, it might seem easier to sample all cluster sizes in one run, but it can be shown that this is not the case,[21] mainly because such a simulation would take too long. Instead we split the simulation into a number of smaller simulations that were restricted to sample a sequence of narrow, but overlapping windows of different cluster sizes. In practice it turned out that it is best to sample only about 15

different cluster sizes in one window, to ensure high accuracy. This implies that the sequence of minima needed to be placed in steps of 10, $n_0=10, 20,...$, up to sizes slightly larger than critical cluster size.

In addition we implemented the parallel tempering scheme of Geyer and Thompson.[22] The main reason for using this scheme is that stacking rearrangements in the nuclei are very slow. With the parallel tempering scheme the phase space can be sampled more efficiently. The idea is to run all the simulations in the different windows in parallel and allow them to exchange clusters between adjacent windows.

To illustrate this, we consider again the example of the hard-sphere system. In this case we needed to calculate the Gibbs free energy of a cluster up to a size of about $n=170$. We therefore split the simulations into 16 windows, where the sequence of minima was placed in steps of 10, $n_0=10, 20,...,160$. In order to obtain the 16 starting configurations we grew clusters from the liquid. We always started from the liquid, applying the bias potential with $n_0=10$. Every time a cluster was stabilized, the minimum n_0 was increased in steps of 10. In the parallel tempering simulation we started all simulations at the same time, but stopped them after five trajectories, to allow neighboring windows to exchange clusters. Before that, we need to decide which sequence we should use to change, either the windows $n_0=10$ with 20, 30 with 40, and so on, or the sequence 20 with 30, 40 with 50, and so on. This was done by generating a random number. The actual change between windows i, j is accepted according to $\exp[-\beta(w_n-w_o)]$, where $w_o=k_i/2(n_i-n_{0,i})^2+k_j/2(n_j-n_{0,j})^2$ is the energy of the biasing potential before and $w_n=k_i/2(n_j-n_{0,i})^2+k_j/2(n_i-n_{0,j})^2$ after the change. In practice it is more convenient to exchange the minima of the bias potential rather than configurations. This requires much less communication between different computer nodes. As a result, each initial configuration is able to reach in principle all cluster sizes in course of the simulation. In Fig. 5 we show the cluster sizes sampled during one simulation for three configurations, which started with cluster sizes $n_0=20$, 50, and 110. The value for the constant of the bias potential was $k_n=k=0.15$ in all windows. As in the unbiased run, the length of one trajectory was 20 moves per particle, plus about 10 volume moves, and in total we performed 100 000 trajectories.

In Fig. 6 we show the results for the Gibbs free energy of a nucleus obtained from the simulations in each window (unbiased+biased runs). The Gibbs free energies in the different windows are determined up to a constant $\Delta G_i(n)/k_BT+b_i$, where the subscript i indicates the number of the window. In order to determine the constants b_i we fitted all the free energy estimates in the different windows to one polynomial in n. This can be done by a linear least-square fit, where we minimize

$$\chi=\sum_{n=1}^{n_{\max}}\left\{\sum_{i=1}^{n_w} w_i(n)\left[\Delta G_i(n)-\sum_{k=1}^{k_{\max}} a_k n^k-b_i\right]^2\right\}.$$

Here $w_i(n)=1/\sigma^2_{\Delta G_i(n)}$ is the statistical weight determined by the variance $\sigma^2_{\Delta G_i(n)}$ of the free-energy measurement and n_w the total number of windows used in the simulation. The maximum order of the polynomial used was $k_{\max}=10$. The linear least-square fit can be performed by using the algorithms in Ref. 23. Note that by using a high-order polynomial, we do not assume a functional form of the nucleation barrier (the barrier might or might not be correctly described by CNT). From the unbiased simulation we get the absolute Gibbs free energy for the formation of a cluster of size n with respect to the liquid state. Therefore the constant b_1 is known. In Fig. 7 we show the final result for the calculation of a nucleation barrier for hard spheres at pressure $\beta P\sigma^3=16$.

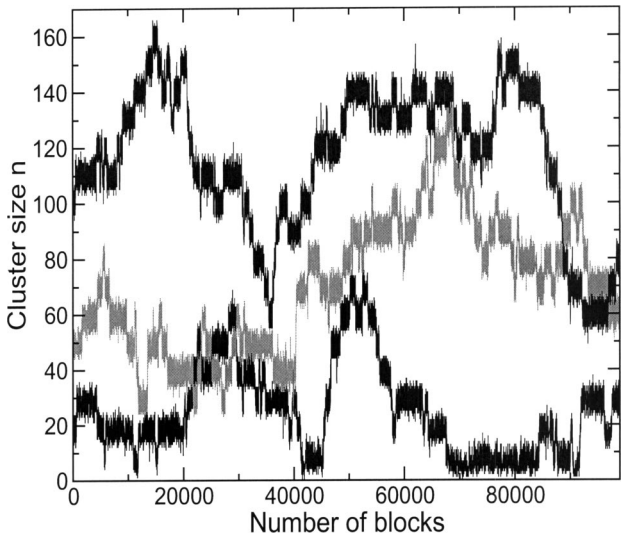

FIG. 5. Examples of the cluster size sampled during one simulation. The different configurations started with clusters of sizes $n=20$, 50, and 110. Due to the parallel tempering technique, swapping between different windows is possible and the configurations could sample almost all possible cluster sizes.

4. Results and discussion

We performed Monte Carlo simulations in the isobaric–isothermal ensemble (NPT) to compute the crystal nucle-

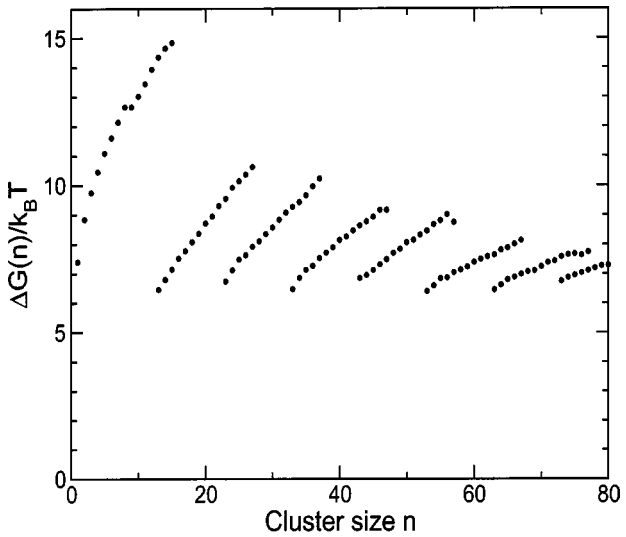

FIG. 6. Sequence of measured Gibbs free energies $\Delta G_i(n)/k_BT+b_i$ from Monte Carlo Simulations in a system of hard spheres in different windows.

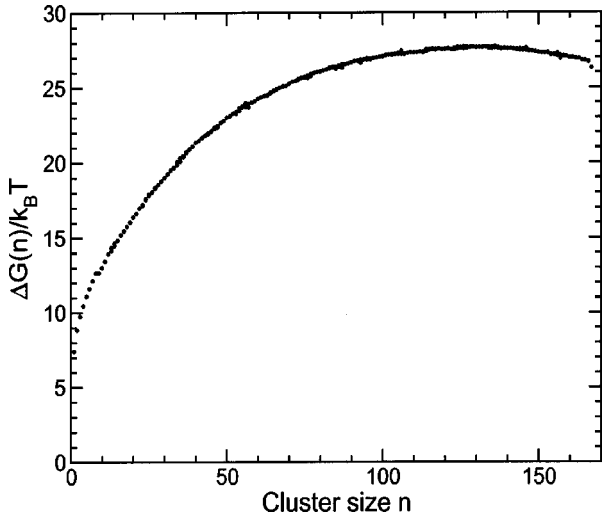

FIG. 7. Gibbs free energy for the formation of a cluster of n hard spheres, after fitting the results for the free energy in the different windows to one polynomial.

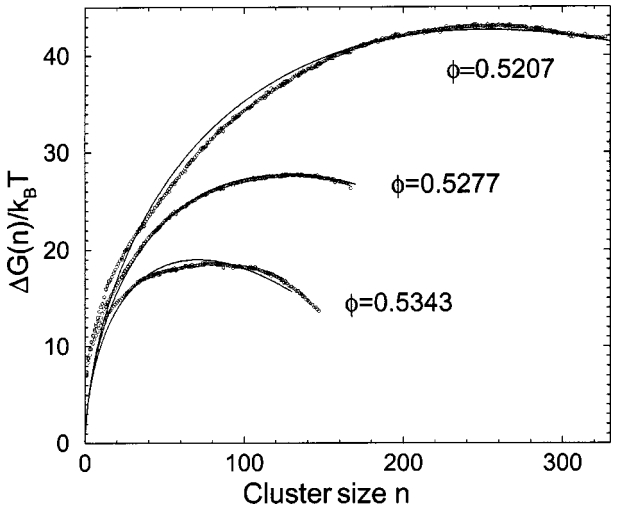

FIG. 8. Calculated free energy barrier for homogeneous crystal nucleation of hard-sphere colloids. The results are shown for three values of the volume fraction. The drawn curves are fits to the CNT expression Eq. (1). The fits yield the following values: $\gamma_{\mathrm{eff}}(P=15)=0.71$, $\gamma_{\mathrm{eff}}(P=16)=0.737$, and $\gamma_{\mathrm{eff}}(P=17)=0.751$.

ation barrier at three different pressures $\beta P\sigma^3=15$, 16, 17. The corresponding bulk volume fractions of the liquid are $\phi=0.5207$, 0.5277, 0.5343. These state points correspond to the lower range of supersaturations where hard-sphere nucleation has been studied experimentally. The reason for selecting this density regime is that at higher supersaturation the system starts to crystallize spontaneously on the time scale of the simulation. Moreover, under those conditions, the assumption of steady-state nucleation is no longer justified, as nuclei will interact with other nuclei almost as soon as they are formed. At lower supersaturation the critical nucleus size becomes very large and the nucleation barrier very high. This has two consequences, one experimental and one numerical. Experimentally, nucleation events in this regime become extremely rare. Numerically, very large system size are needed to study nucleation in this regime. For both reasons, we decided not to simulate nucleation events in this regime. The details of the simulation are as described before and the results are shown in Fig. 8. As expected, with increasing volume fraction the crystal nucleation barrier decreases. Our simulation results for the crystal nucleation barrier can be compared directly to the predictions from CNT for the nucleation barrier, Eq. (1), or the barrier height, Eq. (2). For the hard-sphere system the chemical potential difference can be calculated accurately using phenomenological equations of state for the liquid and the solid. The details are described in Appendix B and the results are shown in Table I. As the solid–liquid interfacial free energy γ of a small crystal nucleus in a supersaturated liquid is not known *a priori* we use its corresponding value for a flat interface at coexistence. This value has been calculated in a recent simulation[13] for three different crystal planes. Here we use $\gamma_{\mathrm{av}}=0.61k_BT/\sigma^2$ which is the average of the three crystal planes. The results for the barrier height in order of increasing density are $\Delta G_{\mathrm{crit}}/k_BT=27$, 15.7, 10.2. These values are about 30%–50% lower than our numerical estimate. This discrepancy might be due to the fact that for a small nucleus in a supersaturated liquid the interfacial free energy is different from that of a flat interface at coexistence. For this reason we also used γ as a fit parameter to our results. Using $R=(3n/(4\pi\rho_S))^{1/3}$ we fitted Eq. (1) to our data. The result can be seen as the solid line in Fig. 8. As can be seen, the functional form of the nucleation barrier seems to be described well by CNT, but the values for the fit parameter $\gamma_{\mathrm{eff}}(P=15)=0.71k_BT/\sigma^2$, $\gamma_{\mathrm{eff}}(P=16)=0.737k_BT/\sigma^2$, and $\gamma_{\mathrm{eff}}(P=17)=0.751k_BT/\sigma^2$ are higher than the coexistence value and they increase with volume fraction. If we assume that this dependence is linear, than our simulation results extrapolate to a value of $\gamma_{\mathrm{eff}}(P=11.7)=0.64k_BT/\sigma^2$ at coexistence. For a detailed discussion of the dependence of the surface free-energy density on the size of the crystal nucleus, see Ref. 24. In Appendix C we discuss an alternative, thermodynamic route to compute the surface free-energy density for the critical nucleus which yields the same results as our estimate for the surface free-energy density from above.

Our results for the surface tension can also be compared to the values extracted from experiments. As already mentioned in the introduction, Palberg[12] fitted the data from Harland and van Megen[7] and obtained $\gamma=0.5k_BT/\sigma^2$ and for the data from Heymann *et al.*[11] he found $\gamma=0.54k_BT/\sigma^2$. These values seem to be rather low. As in the

TABLE I. Summary of the simulation results for the calculation of the nucleation rate for monodisperse hard-sphere colloids. Here ϕ is the volume fraction of the liquid phase. $\Delta G(n_{\mathrm{crit}})$ is the measured free energy to form a cluster of critical size n_{crit}. $f^+_{n_{\mathrm{crit}}}/D_0$ is the attachment rate of particles to the critical cluster divided by the free diffusion coefficient. $I^*=I\sigma/D_0$ is the reduced nucleation rate and λ is the estimated typical jump distance from the calculation of the attachment rate. $\Delta\mu$ is the difference in chemical potential between the two phases.

ϕ	$\Delta G(n_{\mathrm{crit}})$	n_{crit}	$f^+_{n_{\mathrm{crit}}}/D_0$	$\log_{10}[I^*]$	λ	$\Delta\mu$
0.5207	43.0	260	189	−19.3	0.31	0.34
0.5277	27.8	130	43	−13.5	0.46	0.44
0.5342	18.5	75	66	−9.14	0.27	0.54

experiments the particles used had a size polydispersity of about 5% we repeated our simulations for a suspension with 5% polydispersity. We find that both systems have the same nucleation barrier at the same $\Delta\mu$.[25] Therefore polydispersity cannot explain the discrepancy. Note that in our simulations of the polydisperse system we used the semigrand ensemble. This implies that the difference in chemical potential in the two phases is equal for all particle radii and the interpretation of our barrier calculations with CNT is well defined, see also Appendix C.

B. Calculation of the kinetic prefactor

1. General approach

In atomistic simulations, the kinetic prefactor is usually calculated using the Bennett–Chandler scheme.[26] In the case where the barrier crossing is relatively diffusive, it is attractive to use a modification proposed by Ruiz-Montero *et al.*[27] The principle of both methods is to generate a large number of independent configurations at the top of the barrier. These configurations are then used as the starting point for an unbiased trajectory in which one determines if the nucleus grows and the system crystallizes, or if it shrinks. From the number of nuclei that grow and shrink one can extract the kinetic factor. However, in order to get a reasonable estimate one has to simulate a rather large number of trajectories. Ten Wolde *et al.*[28] applied the approach of Ref. 27 to calculate the gas–liquid nucleation rate in a Lennard-Jones system. Using over 300 trajectories of about 5000 time steps each, the resulting value for the transmission coefficient still had a relative error close to 100%. The reason is that the barrier-crossing process in a nucleation event is effectively, purely diffusive. Fortunately, in that limit, we can compute the kinetic prefactor directly using the expression: $\kappa = Z\rho_{\mathrm{liq}} f^{+}_{n_c}$, where $f^{+}_{n_{\mathrm{crit}}}$ is the attachment rate of particles to the critical cluster. The Zeldovich factor Z is already known from the barrier calculation. In order to compute $f^{+}_{n_{\mathrm{crit}}}$, we assume that the critical cluster grows and shrinks via the diffusive attachment of single particles. We can then define an effective diffusion constant for the change in critical cluster size,

$$D^{\mathrm{att}}_{n_{\mathrm{crit}}} = \frac{1}{2}\frac{\langle \Delta n^2_{\mathrm{crit}}(t)\rangle}{t}.$$

Here $\Delta n^2_{n_{\mathrm{crit}}}(t) = [n_{\mathrm{crit}}(t) - n_{\mathrm{crit}}(t=0)]^2$ is the mean square change in the number of particles in the critical cluster. As the slope of this change is related to the corresponding attachment rates via $\langle \Delta n^2_{\mathrm{crit}}(t)\rangle/t = (f^{+}_{n_{\mathrm{crit}}} + f^{-}_{n_{\mathrm{crit}}})/2$, and as we know that, at the top of the barrier, the forward and backward rates are equal $f^{+}_{n_{\mathrm{crit}}} = f^{-}_{n_{\mathrm{crit}}}$, we get

$$f^{+}_{n_{\mathrm{crit}}} = \frac{1}{2}\frac{\langle \Delta n^2_{\mathrm{crit}}(t)\rangle}{t}. \tag{9}$$

This is a general expression for the calculation of the kinetic factor for diffusive barrier crossing. Using a molecular dynamics simulation one only needs to measure the change in size of the critical cluster as a function of time. The only restriction is that, during the measurement, the critical nucleus needs to fluctuate around its critical value. One therefore needs to run a couple of trajectories and select the data where this is the case. In the next section we show how we applied this method to a system of hard-sphere colloids.

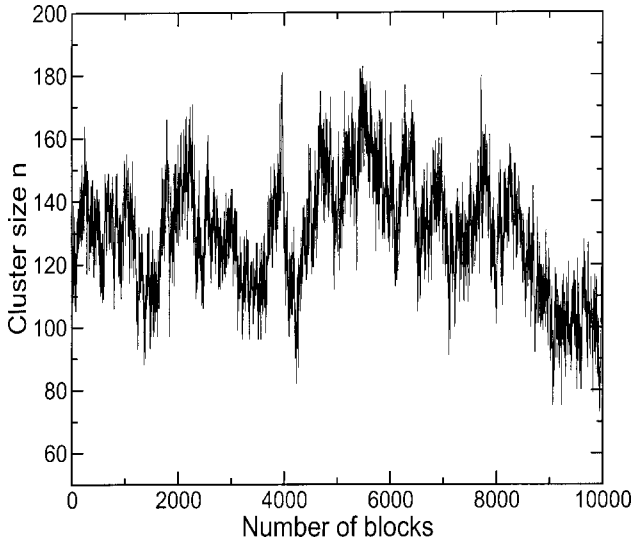

FIG. 9. The development of the size n of the critical cluster during one trajectory at volume fraction $\phi = 0.5277$. Here one block is 100 moves per particle in an *NVE* Monte Carlo simulation. Note in particular the fluctuations of the cluster size about its critical value.

2. Application to hard colloidal spheres

In principle, it is straightforward to apply the above method to the calculation of a kinetic factor for crystal nucleation. However, in the case of hard colloidal spheres one needs to have a simulation method that generates trajectories following Brownian dynamics, and the effect of hydrodynamic interactions also needs to be considered. Trajectories following Brownian dynamics could be generated using a kinetic Monte Carlo scheme proposed by Hinson and Cichocki.[29] These authors show that, in the limit of very small maximum particle displacement, $\Delta x_{\mathrm{max}} \to 0$, the trajectories generated by the kinetic Monte Carlo simulation are stochastically equivalent to the process described by the Smoluchowski equation. The limit $\Delta x_{\mathrm{max}} \to 0$ means that simulation time would become infinitely long. However, Hinson and Cichocki also propose an extrapolation procedure with which this limit can be approached systematically by repeating simulations with a smaller maximum displacement.

In experiments nucleation rates are usually presented in dimensionless form $I^* = I\sigma^5/D_0$, where σ is the diameter of a monomer and D_0 the free diffusion coefficient. Therefore we only need to compute the ratio $f^{+}_{n_{\mathrm{crit}}}/D_0$. First we computed the nucleation barrier using a biased *NPT* Monte Carlo simulation. From these simulations we could determine the critical cluster size and had generated independent configurations in which such a cluster was stabilized. We used these configurations, to perform an unbiased kinetic *NVE* Monte Carlo simulation, measuring the size of the critical cluster as a function of Monte Carlo blocks. In Fig. 9 we show such a measurement at $\phi = 0.5277 (P = 16)$. From these data we then extracted the attachment rate using Eq. (9)

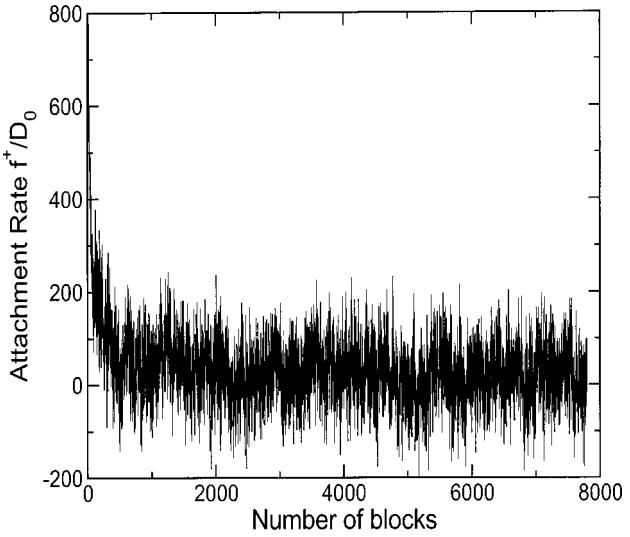

FIG. 10. Attachment rate of particles to the critical cluster at volume fraction $\phi=0.5277$. The attachment rate for short times is much higher than for long times. As the diffusion time of a cluster over the nucleation barrier is in the range of the long time behavior of the attachment rate, this value has to be used.

(see Fig. 10). Surprisingly, we see that the attachment rate has a different short-time and long-time behavior. This implies that, at short times, the diffusion in cluster size is not a Markov process. As the diffusion of the critical cluster over the nucleation barrier is on the time scale of the long-time behavior of the attachment rate, this is the value we have to use. To test the dependence of our results on the maximum particle displacement we performed simulations for two different values $\Delta x_{\max}=0.12\sigma$ and 0.012σ. The corresponding values for the free diffusion coefficients are $D_0=\langle\Delta x_{\max}^2\rangle/6$. The ratio of the results for $f_{n_{\text{crit}}}^+/D_0$ in both simulations is equal to 4.79. Computing the long-time self-diffusion coefficient $D_S^L/D_0=\langle(r(0)-r(t))^2\rangle/6tD_0$ we get a ratio in both simulations of 5.07. Therefore the difference in the results for the attachment rate is mainly due to diffusion. In our simulations we did not follow the extrapolation procedure for $\Delta x_{\max}\to 0$ described in Ref. 29, as for $\Delta x_{\max}=0.012\sigma$ we are already in a limit where the attachment rate has effectively reached its limiting value. We justify this by testing our approach on the calculation of the long-time self-diffusion coefficient, which will be discussed later. So far in our simulations we did not take hydrodynamic interactions into account. However, these are certainly important in dense colloidal suspensions. As proposed by Medina-Noyola,[30] we corrected for this effect by replacing the free diffusion coefficient D_0 by the short-time self-diffusion coefficient D_S^S. We therefore have to multiply our result by a factor $\alpha=D_S^S/D_0$. There are several rather similar functional forms for this factor proposed in the literature. Here we used the phenomenological expression $(1-\phi/0.64)$[1.17,31] where ϕ is the volume fraction. As a test of our approach, we computed the reduced long-time self-diffusion coefficient D_S^L/D_0. Our results, $D_S^L/D_0=2.9\times10^{-3}$, 2.5×10^{-3}, 2.1×10^{-3}, calculated at volume fractions $\phi=0.5207$, 0.5277, 0.5342, are within statistical error of experimental data, see e.g., Refs. 32 and 33. For the calculation of the kinetic factor we usually performed about five trajectories. The length of the trajectory depends on whether the cluster size fluctuates around the critical size or not; if not the simulation is stopped. From these simulations we calculated the attachment rate. The error estimates vary between a factor of 1 for the larger critical cluster sizes and a factor of 2 to 3 for the smaller cluster sizes. In the regime of smaller critical cluster sizes, the fluctuations in cluster size are almost on the order of the critical cluster size and it becomes therefore more difficult to get a good estimate. To compare the efficiency of our scheme with the previous one we need to compare the number of trajectories to run, but also the absolute length of the trajectory itself. The latter is difficult to compare as different systems were simulated with different algorithms. However, as the number of trajectories we used is about two orders of magnitude fewer the power of our scheme is clear.

3. Results and discussion

The results of our calculations of the attachment rate for the monodisperse hard-sphere system are summarized in Table I. As experimentally determined values for the kinetic factor often differ by orders of magnitude from those predicted by CNT it is important to compare our numerically computed kinetic factor with the ones predicted by CNT. From the calculation of the nucleation barrier we saw that the functional form of the nucleation barrier can be fitted accurately to the corresponding analytical expression from CNT. The prediction of the Zeldovich factor from our numerical calculations and CNT are therefore almost identical. The remaining quantity to compare is the reduced attachment rate. Using Eq. (5) it is given by

$$f_{\text{CNT}}^+/D_0=24(D_S/D_0)n_{\text{crit}}^{2/3}/\lambda^2.$$

If we assume that $D_S=D_S^L$, where D_S^L is the long-time diffusion constant, and treat λ as a fit parameter to reproduce our calculated attachment rates, we get values between $\lambda\approx0.27$–0.46σ (see Table I). This is in the order of the interparticle spacing and therefore close to what we would expect for a typical jump distance. In contrast to that, experimental estimates yield values $\lambda=2.8$–17σ[12]. The identification $D_S=D_S^L$ is justified by the fact that the time λ^2/D_S^L corresponds to long-time diffusion.

Our simulation results for the nucleation barrier and the kinetic prefactor allow us to predict the nucleation rates which can be directly compared to experiments without adjustable parameter. In Fig. 11 we show our numerical predictions for the reduced nucleation rate for a monodisperse suspension and a suspension with 5% polydispersity. The latter results can be compared directly to the experiments. Note that the polydispersity in Ref. 8 is about 2.5%. As can be seen from the figure, the dependence of the nucleation rates on the density of the system is much more pronounced in the simulations than in the experiments. This discrepancy between the simulations and experiment is unexpected and significant because hard-sphere colloids are among the best studied experimental realizations of a simple liquid. We know the structural and thermodynamic properties of hard-

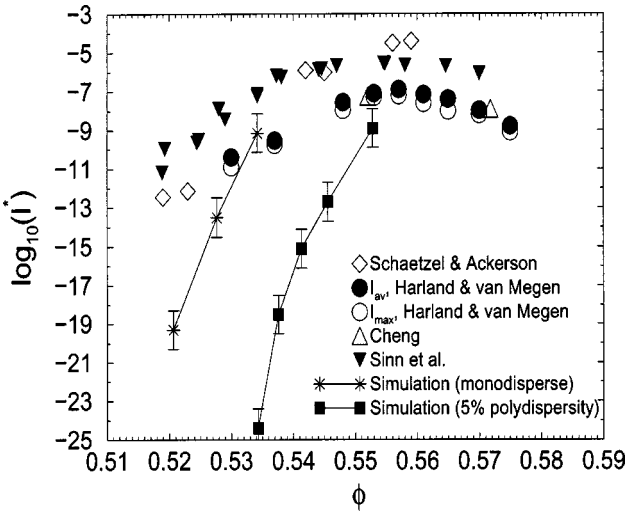

FIG. 11. Reduced nucleation rates $I^*=I\sigma^5/D_0$ as a function of the volume fraction of the metastable liquid. The simulation data for monodisperse colloids are indicated by the *—the drawn curve joining the simulation points is meant as a guide to the eye. In the same figure we show the experimental results of Ref. 6 (◇), Ref. 7 (○ and ●), Ref. 32 (△), and Ref. 8 (▼). We also performed simulations on model systems that have the same polydispersity (5%) as the experimental systems. These simulation results are denoted by the filled squares.

sphere suspensions quite accurately and, more significantly, these properties tend to be well reproduced by the ideal, hard-sphere model. Hence, large discrepancies between experiment and simulation cannot be easily dismissed as being due to uncertainties in the parameters that characterize the colloidal suspension. Rather, we must envision the possibility that either our theoretical description of crystallization is inadequate or that what is measured is not really the steady-state, homogeneous nucleation rate. In fact, the latter suggestion is not altogether unreasonable, as light-scattering cannot be used to see the very early stages of crystal nucleation. Second, the experiments are extremely sensitive to any residual ordering in the solution that may have survived the preparation of the experimental system. More experiments (and simulations) may be needed to resolve this issue.

IV. CLUSTER ANALYSIS

Our simulation techniques also allow us to study the formation of small crystal nuclei in detail. This is interesting as already in 1897 Ostwald[34] pointed out the role of metastable phases in crystal nucleation when he formulated his famous step rule. This rule states that the phase that nucleates does not need to be the one that is thermodynamically most stable. In the recent years there have been several attempts to provide a microscopic explanation[35,36] for Ostwald's observation. Alexander and McTague[35] argue, on the basis of Landau theory, that if the differences in the liquid and solid densities were not too great, then the phase that would be nucleated from the liquid would be bcc regardless of the structure of the stable (lowest free energy) phase. Klein and Leyvraz,[36,37] showed that for deeply quenched systems with long-range interactions, the critical droplet can have a bcc symmetry, but does not have a bcc crystalline structure. Simulations by ten Wolde *et al.*[18] showed that the situation can even be more subtle, at least for a Lennard-Jones system: The core of a stable Lennard-Jones cluster formed a stable fcc structure while the surface of the nucleus showed indications of a bcc structure. Thermodynamically the formation of metastable phases might be explained by differences in interfacial free energies. The formation of a bcc-liquid interface might cost less energy than that of a fcc-liquid interface. In the case of hard spheres it is known that the fcc phase is the stable structure, but the free energy difference between the fcc and the hcp structure is very small ($<10^{-3}k_BT$).[38,39] This means that thermal fluctuations of the order of k_BT could transform a cluster of 1000 particles from fcc to hcp or just cause stacking faults. Note that the fcc and the hcp structure differ only in the stacking of close-packed hexagonal crystal planes. For the fcc structure the stacking is ABC, whereas for the hcp structure the stacking is AB. If the interfacial free energies of a crystal fcc-liquid, hcp-liquid or a rhcp-liquid interface are different, than this could also completely change this picture. Here rhcp refers to a random stacking of the close-packed hexagonal crystal planes. The question if small crystal nuclei are more fcc or hcp like is not clear.

Experiments by Pusey *et al.*[40] and Elliot *et al.*[41] indicate that the fcc structure is favored. Whereas in the microgravity experiments by Zhu *et al.*[42] they found that small nuclei have a rhcp structure. To resolve this question we analyzed the structure of small nuclei that were generated in our simulations. From a direct inspection of the nuclei we found that the structure of the nuclei is rhcp (see Fig. 12). In order to be able to carry out the stacking analysis the nuclei needed to have a size of at least 150 particles, otherwise the number of layers is too small. To study the structure of even smaller nuclei we performed a local bond-order analysis as described in Sec. III A 1. We set up a set of vectors, $\mathbf{v}_{\mathrm{rhcp}}$, $\mathbf{v}_{\mathrm{bcc}}$, $\mathbf{v}_{\mathrm{ico}}\mathbf{v}_{\mathrm{liq}}$, which contain the characteristic distribution functions of the relevant lattice structures, i.e., rhcp, bcc, ico, and the liquid structure, see also Fig. 2. In our simulation the distribution functions for the cluster were also calculated. The corresponding vector is $\mathbf{v}_{\mathrm{cl}}$. The vector $\mathbf{v}_{\mathrm{cl}}$ was then decomposed by minimizing the difference Δ,

$$\Delta=\{\mathbf{v}_{\mathrm{cl}}-(f_{\mathrm{rhcp}}\mathbf{v}_{\mathrm{rhcp}}+f_{\mathrm{bcc}}\mathbf{v}_{\mathrm{bcc}}+f_{\mathrm{ico}}\mathbf{v}_{\mathrm{ico}}+f_{\mathrm{liq}}\mathbf{v}_{\mathrm{liq}})\}^2.$$

The coefficients f_{rhcp}, f_{bcc}, f_{ico}, f_{liq} are a measure for the type of order in the system. If we apply this analysis to an equilibrated bcc crystal, we would get $f_{\mathrm{bcc}}=1$ and zero for the others. In Fig. 13 we show the results for f_{rhcp}, f_{bcc}, f_{ico}, and f_{liq} as a function of the size of the largest cluster in the system at $P=15$. The results for $P=16$ are qualitatively similar. The figure shows that bcc and icosahedral structures play no role in the nucleation process. Small clusters are fairly disordered and have an appreciable liquidlike signature. The figure shows that the rhcp signature is dominant for all cluster sizes.

V. CONCLUSIONS

As should be clear from the preceding sections, special numerical techniques are needed to study homogeneous crystal nucleation under "experimental" conditions. We described these techniques in some detail, in order that the

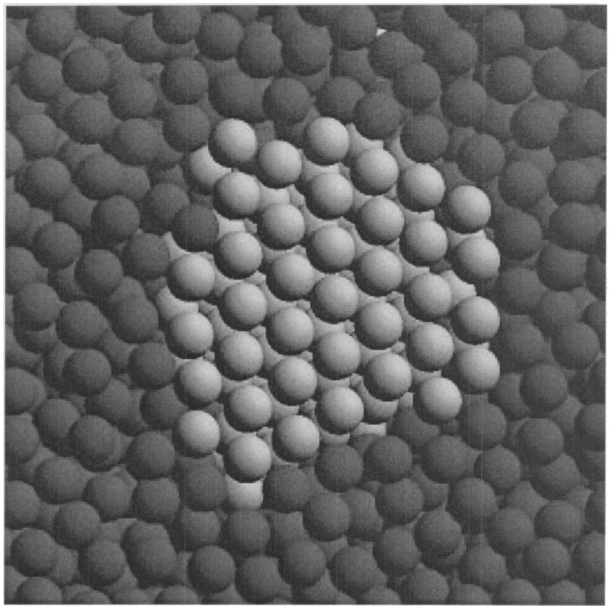

FIG. 12. Snapshot of a cross section of a critical nucleus of a hard-sphere crystal at a liquid volume fraction $\phi=0.5207$. The figure shows a three-layer thick slice through the center of the crystallite. Solidlike particles are shown in light gray (yellow) and liquid-like particles in dark gray (blue). The layers shown in the figure are close-packed hexagonal crystal planes. The stacking shown in this figure happens to be fcc-like, i.e., ABC stacking—however, analysis of many such snapshots showed that fcc and hcp stackings were equally likely.

reader may assess their validity. We stress that the techniques described in this paper are not ''merely'' numerical recipes. On the contrary, in all cases, the physical approximations behind the techniques are of crucial importance. Therefore, this paper focuses more on the physics of nucleation than on the numerics. The examples that we describe in this paper have been included for two reasons: (a) to illustrate the use of the techniques that we describe and (b) to provide more detailed tabular material than could be included in earlier brief communications.[9,25]

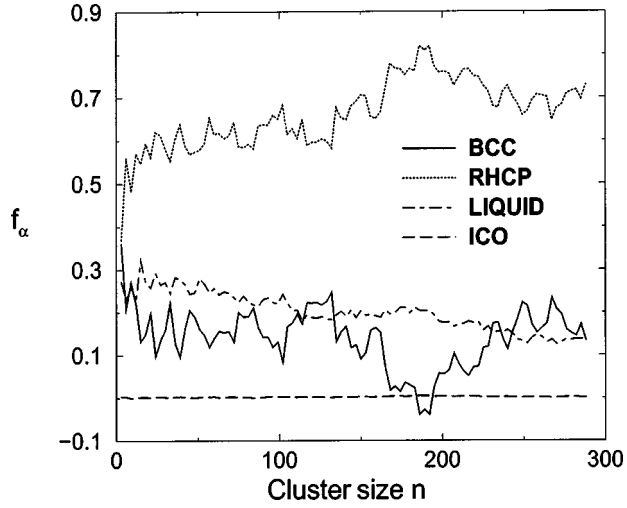

FIG. 13. Structure analysis of (pre)critical crystal nuclei. The figure shows the relative weight of the structural signatures for rhcp, bcc, icosahedral, and liquidlike ordering in hard-sphere crystal nuclei of size *n*.

We wish to stress that the methods described in this paper are not fully satisfactory for several reasons. First of all, it is one of our aims to investigate the pathway for crystal nucleation. Ideally, such a study should be performed without making any *a priori* assumptions about the order parameters that can act as ''reaction coordinates.'' In fact, the approach proposed by Chandler and co-workers[43] provides, in principle, such an unbiased scheme. However, for the present problem, we were thus far unable to implement that scheme in a way that would not be prohibitively costly.

Second, we should caution the reader against a too literal interpretation of the nucleation barriers that we determine. A different choice of order parameters would have resulted in a different shape of the nucleation barrier. However, its height should hardly be sensitive to this choice. Most importantly, the absolute nucleation rate, i.e., the one object that can be determined unambiguously in experiments, should not depend at all on our choice of order parameter. A poor choice of order parameters will make our simulations very inefficient but, given enough computing power, the resulting nucleation rate should still be correct.

ACKNOWLEDGMENTS

We thank T. Schilling and C. Valeriani for a critical reading of the paper. We also thank T. Palberg for permission to show Fig. 1 and for his comments on the paper. This work was supported by the Division of Chemical Sciences (CW) of the Netherlands organization for Scientific Research (NWO). The work of the FOM Institute is part of the research program of FOM, and is made possible by financial support from NWO.

APPENDIX A: DISTRIBUTION OF CLUSTER SIZES IN EQUILIBRIUM

The distribution of cluster sizes can be derived microscopically from statistical mechanics. The derivation is based on Refs. 14, 15, and 19. The partition function of a system containing N particles in a volume V at temperature T is given by

$$Q(N,V,T)=\frac{1}{\Lambda^{3N}N!}\int d\mathbf{r}^N \exp[-\beta U(\mathbf{r}^N)].$$

Here $U(\mathbf{r}^N)$ is the potential energy of the configuration with coordinates $\mathbf{r}^N$ and $\Lambda=h/\sqrt{2\pi mkT}$ is the thermal de Broglie wavelength. Now we assume that we have a criterion, that enables us to identify a cluster in our system. We then define a function $w_n(\mathbf{r}^n)$ such that

$$w_n(\mathbf{r}^n)=\begin{cases}1 & \text{if all } n \text{ particles belong to the cluster,}\\ 0 & \text{otherwise.}\end{cases}$$

In addition, we define a function $w_r(\mathbf{r}^N)=\Pi_{i=n+1}^{N}[1-w_{n+1}(\mathbf{r}^n,\mathbf{r}_i)]$, which ensures that all other particles do not belong to the cluster

$$w_r(\mathbf{r}^N)=\begin{cases}1 & \text{if no other particle belongs to the cluster,}\\ 0 & \text{if any other particle belongs to the cluster.}\end{cases}$$

We can then define a partition function for a system that contains at least one n-particle cluster

$$Q_n(N,V,T)=\frac{1}{\Lambda^{3n}n!}\frac{1}{\Lambda^{3(N-n)}(N-n)!}\times\int d\mathbf{r}^n\int d\mathbf{r}^{N-n}\,w_n(\mathbf{r}^n)w_r(\mathbf{r}^N)\times\exp[-\beta U(\mathbf{r}^n,\mathbf{r}^{N-n})],$$

where we have used the fact that there are $N!/(n!(N-n)!)$ ways to select an n-particle cluster. Note that the remaining particles may still form additional clusters of size n. The product $w_n(\mathbf{r}^n)w_r(\mathbf{r}^{N-n})=1$, only if all $\mathbf{r}^n$ particles belong to the specified cluster and all the other $\mathbf{r}^{N-n}$ do not. We now rewrite the potential energy of the system as the sum of contributions from the particles in the cluster $U_n(\mathbf{r}^n)$ and the contribution from all other particles $U_{N-n}(\mathbf{r}^{N-n})$, plus the contribution from the interactions between particles in the cluster and the others $U_{n,N-n}(\mathbf{r}^n,\mathbf{r}^{N-n})$. The partition function then becomes

$$Q_n(N,V,T)=\frac{1}{\Lambda^{3n}n!}\frac{1}{\Lambda^{3(N-n)}(N-n)!}\times\int d\mathbf{r}^{N-n}\exp[-\beta U_{N-n}(\mathbf{r}^{N-n})]\times\int d\mathbf{r}^n\,w_nw_r\exp[-\beta U_n(\mathbf{r}^n)]\times\exp[-\beta U_{n,N-n}(\mathbf{r}^n,\mathbf{r}^{N-n})].$$

We can now define effective potentials for all the particles in the cluster

$$U_n'=U_n-kT\ln[w_n],$$

and the interaction between cluster particles and the others

$$U_{n,N-n}'=U_{n,N-n}-kT\ln[w_r],$$

yielding

$$Q_n(N,V,T)=\frac{1}{\Lambda^{3(N-n)}(N-n)!}\frac{1}{\Lambda^{3n}n!}\times\int d\mathbf{r}^{N-n}\exp[-\beta U_{N-n}(\mathbf{r}^{N-n})]\times\int d\mathbf{r}^n\exp[-\beta U_n']\exp[-\beta U_{n,N-n}'].$$

Multiplication of the right-hand side by $Q(N-n,V,T)/Q(N-n,V,T)$ gives

$$Q_n(N,V,T)=\frac{1}{n!\Lambda^{3n}}Q(N-n,V,T)\times\int d\mathbf{r}^n\langle\exp[-\beta U_{n,N-n}']\rangle\exp[-\beta U_n'],\tag{A1}$$

where we have defined a potential of mean force

$$\langle\exp[-\beta U_{n,N-n}']\rangle=\frac{\int d\mathbf{r}^{N-n}\exp[-\beta U_{n,N-n}']\exp[-\beta U_{N-n}(\mathbf{r}^{N-n})]}{(N-n)!\Lambda^{3(N-n)}Q(N-n,V,T)}.$$

It is the average potential the particles in the cluster feel due to the interactions with all other particles. We define now the partition function of an n-mer as

$$q_n(V,T)=\frac{1}{n!\Lambda^{3n}}\int d\mathbf{r}^n\langle\exp[-\beta U_{n,N-n}']\rangle\exp[-\beta U_n'].\tag{A2}$$

Note that $q_n(V,T,\mu)$ is the partition function of a cluster in which the interaction with the remaining $(N-n)$ molecules is included in the factor $\langle\exp[-\beta U_{n,N-n}']\rangle$. The interaction with possible other clusters is also included as such clusters can still exist in the remaining $(N-n)$ particles. The partition function Eq. (A1) can then be written as

$$Q_n(N,V,T)=Q(N-n,V,T)q_n(V,T).$$

The probability to find at least one cluster of size n is then given by

$$P_n=\frac{Q_n(N,V,T)}{Q(N,V,T)}=\frac{Q(N-n,V,T)}{Q(N,V,T)}q_n(V,T).$$

As the free energy of the system is given by $F=-kT\ln[Q]$, the above equation becomes

$$P_n=q_n(V,T)\exp[-\beta(F(N-n,V,T)-F(N,V,T))].$$

Using

$$F(N-n,V,T)\approx F(N,V,T)-\left(\frac{\partial F}{\partial N}\right)_{V,T}n$$

it follows that

$$P_n=q_n(V,T)\exp[+\beta\mu n].$$

The problem with this definition of the probability is that it depends on the volume V. To see this we rewrite Eq. (A2)

$$q_n(V,T)=\frac{1}{n!\Lambda^{3n}}\int d\mathbf{r}^n\exp[-\beta U_{\text{eff}}],$$

where we defined an effective potential $U_{\text{eff}}=\langle U_{n,N-n}'\rangle+U_n'$. Rewriting the partition function in terms of the center of mass of the cluster yields

$$q_n(V,T)=\frac{n^3}{n!\Lambda^{3n}}\int dR_{CM}\int d\mathbf{r}'^{n-1}\exp[-\beta U_{\text{eff}}].$$

Performing the integral over the center of mass and defining a partition function of the cluster in terms of the internal coordinates we get

$$q_n=\frac{V}{\Lambda_n^3}\times q_n^{\text{internal}},$$

where $\Lambda_n=h/\sqrt{2\pi nmkT}$ is the de Broglie wavelength of the cluster and

$$q_n^{\text{internal}} = \frac{n^{3/2}}{\Lambda^{3(n-1)} n!} \int d\mathbf{r}'^{n-1} \exp[-\beta U_{\text{eff}}].$$

It is better to define an intensive probability distribution

$$\frac{P_n}{N} = \frac{1}{\rho \Lambda_n^3} q_n^{\text{internal}} \exp[-\beta \mu n],$$

where ρ is the number density of the system. For rare clusters we can write the probability as

$$P_n = p_n(1) + p_n(2) + \cdots \approx p_n(1), \tag{A3}$$

where $p_n(i)$ is the probability that there are exactly i clusters of size n. If we assume that the formation of different clusters is uncorrelated $p_n(i) = [p_n(1)]^i$, then we can neglect higher order terms provided the probabilities are small, $p_n(1) \ll 1$. As the average number of clusters of size n is equal to

$$N_n = 1 p_n(1) + 2 p_n(2) + 3 p_n(3) + \cdots \tag{A4}$$

we can write in the case of rare clusters

$$\frac{P_n}{N} \approx \frac{N_n}{N} = \frac{1}{\rho \Lambda_n^3} q_n^{\text{internal}} \exp[-\beta \mu n]. \tag{A5}$$

We note that this is a classical result and should not depend on Planck's constant h, and, in fact it does not, as the ideal gas part of the chemical potential

$$\mu = \mu^{\text{ex}} + kT \ln[\Lambda]$$

cancels the h in Λ_n.

The main point of Eq. (A5) is that we can write down a microscopic expression for the equilibrium number of n-clusters if this number, which is equal to the probability of finding one cluster of size n, is much less than one. Using Eq. (6) this in turn defines an intensive Gibbs free energy of the cluster where the reference state is the homogeneous phase,

$$\frac{N_n}{N} = \exp[-\Delta G(n)/k_B T]. \tag{A6}$$

This is the key relation which enables us to compute a nucleation barrier in a Monte Carlo simulation.

APPENDIX B: CALCULATION OF THE CHEMICAL POTENTIAL

Here we describe the calculation of the chemical potential for the monodisperse hard-sphere system. For the calculation of the chemical potential of the two phases, we performed a thermodynamic integration. The Helmholtz free energy F, per particle and in units of the thermal energy $k_B T$, of a liquid is determined by integrating the equation of state, starting from low densities, where the fluid behaves like an ideal gas,[21]

$$\frac{F(\rho)}{N k_B T} = \frac{F^{\text{id}}(\rho)}{N k_B T} + \frac{1}{k_B T} \int_0^\rho d\rho' \left(\frac{P(\rho') - \rho' k_B T}{\rho'^2} \right),$$

where $P(\rho)$ is the pressure and $F^{\text{id}}(\rho)/N k_B T = \ln(\rho) - 1$ the free energy of an ideal gas at density ρ. The corresponding chemical potential is given by

$$\frac{\mu(\rho)}{k_B T} = \frac{F(\rho)}{N k_B T} + \frac{P(\rho)}{\rho k_B T}.$$

The calculation of the chemical potential of the solid is slightly more complicated. The reason is that it is not possible to perform the integration from the ideal gas limit, as the solid melts at lower densities. One has to calculate the excess free energy of a solid at a reference density where the solid is stable, which requires a different thermodynamic integration technique, the so-called Einstein integration. The idea is to transform the solid reversibly into an Einstein crystal, where the atoms are coupled harmonically to their lattice sites. The free energy can be calculated very precisely and we use the results from Polson *et al.*[44] for the excess free energy of a (defect free) hard-sphere solid at coexistence: $F^{\text{ex}}(\rho_{\text{coex}} = 1.0409)/N k_B T = 5.918\,89$. From the above equation we can then calculate the chemical potential of the solid at any other density according to

$$\frac{\mu(\rho)}{k_B T} = \frac{F^{\text{id}}(\rho)}{N k_B T} + 5.918\,89 + \frac{1}{k_B T} \int_{\rho_{\text{coex}}}^\rho d\rho' \times \left(\frac{P(\rho') - \rho' k_B T}{\rho'^2} \right) + \frac{P(\rho)}{\rho k_B T}.$$

For the equation of state $P(\rho)$ we used the analytical expressions by Hall[45] for the liquid and the solid. The integration was performed numerically.

APPENDIX C: SURFACE FREE ENERGIES OF CRITICAL NUCLEI

In general, the value of the surface tension (or, more generally, surface free-energy density) depends on the criterion used to define the surface of a cluster. However, in the special case that we consider a critical nucleus, there exists a thermodynamic relation between the height of the nucleation barrier and the surface free-energy density associated with the thermodynamic surface of tension. Below, we derive this relation.

Consider two systems. System I contains the homogeneous, metastable phase β. System II contains the parent phase (β) in unstable equilibrium with a critical nucleus of phase α. We consider the general case that the parent phase is an n-component mixture. The height of the nucleation barrier can be computed in several ways (depending on the thermodynamic variables that we keep fixed). For instance, for a system at constant pressure and temperature, the nucleation barrier is given by the difference in Gibbs free energy between states II and I. To compute this barrier, we first evaluate the difference in the internal energy

$$\Delta U = U^{\text{II}} - U^{\text{I}}. \tag{C1}$$

The internal energy of system I is given by

$$U^{\text{I}} = T^{\text{I}} S^{\text{I}} - p^{\text{I}} V^{\text{I}} + \sum_{i=1}^n \mu_i^{\text{I}} N_i, \tag{C2}$$

where μ_i^{I} is the chemical potential of component i in state I. As state II is also in equilibrium (be it an unstable one), the chemical potentials of all species are also constant throughout the system—even though the system itself is inhomogeneous. The internal energy of system II is given by

$$U^{\mathrm{II}} = T^{\mathrm{II}}S^{\mathrm{II}} - p_\alpha^{\mathrm{II}}V_\alpha^{\mathrm{II}} - p_\beta^{\mathrm{II}}V_\beta^{\mathrm{II}} + \gamma A + \sum_{i=1}^{n} \mu_i^{\mathrm{II}}N_i$$

$$= T^{\mathrm{II}}S^{\mathrm{II}} + (p_\beta^{\mathrm{II}} - p_\alpha^{\mathrm{II}})V_\alpha^{\mathrm{II}} - p_\beta^{\mathrm{II}}V^{\mathrm{II}} + \gamma A + \sum_{i=1}^{n} \mu_i^{\mathrm{II}}N_i. \qquad \text{(C3)}$$

We consider the situation that the nucleus is formed at constant pressure and temperature. In that case, $p^{\mathrm{I}} = p_\beta^{\mathrm{II}} = p$, $T^{\mathrm{I}} = T^{\mathrm{II}} = T$ and $\mu_i^{\mathrm{I}} = \mu_i^{\mathrm{II}} = \mu_i$. The last equality follows because the chemical potential in the parent phase is a function of P and T only. The difference between the internal energies of systems I and II is then given by

$$\Delta U = T\Delta S + (p - p_\alpha^{\mathrm{II}})V_\alpha^{\mathrm{II}} + \gamma A - p\Delta V, \qquad \text{(C4)}$$

where $\Delta S = S^{\mathrm{II}} - S^{\mathrm{I}}$ and $\Delta V = V^{\mathrm{II}} - V^{\mathrm{I}}$. Note that the terms involving the chemical potentials drop out of the expression for ΔU. The expression for the nucleation barrier then becomes

$$\Delta G = \Delta U + p\Delta V - T\Delta S = (p - p_\alpha^{\mathrm{II}})V_\alpha^{\mathrm{II}} + \gamma A. \qquad \text{(C5)}$$

This equation holds for every dividing surface. Moreover, we have not made any approximations concerning the compressibility of either phase, nor concerning the interfacial free energy. If we choose the surface of tension as the dividing surface, then we can use the Laplace equation ($\Delta p = 2\gamma_s/R_s$) to express the height of the barrier as

$$\Delta G = \frac{4}{3}\pi R_s^2 \gamma_s = \frac{2\pi}{3}\Delta p R_s^3. \qquad \text{(C6)}$$

In what follows, it will turn out to be convenient to express the surface tension γ_s in terms of the barrier height ΔG and the Laplace pressure Δp

$$\gamma_s = \left(\frac{3}{16\pi}\right)^{1/3} \Delta G^{1/3}\Delta p^{2/3}. \qquad \text{(C7)}$$

We stress that, for every component, the chemical potentials in the parent phase and in the critical nucleus are the same. In the absence of the Laplace pressure, the chemical potentials in phase α would be lower than those in phase β. The effect of the Laplace pressure is to compensate this difference for every component i. At first sight, it would seem that the computation of Δp is an intractable problem for a multicomponent system—to satisfy the condition that $\mu_i^\alpha = \mu_i^\beta$ for all i, it is not enough to compress phase α; we should also change its composition. The problem is greatly simplified if we make use of the semigrand canonical ensemble. In the semigrand ensemble, the independent variables that describe the state of an n-component system are: the temperature T, the pressure P, the total number of particles N and the set of $n-1$ differences in the chemical potential ($\Delta\mu_i$) between a reference species (say, species 1) and all other species $i \neq 1$. The number of components n can be infinite.

At coexistence, the chemical potentials of all species i in the two phases, are equal: $\mu_i^\alpha = \mu_i^\beta$. In the notation of the semigrand ensemble, this means that, at coexistence, the temperature and pressure of the two phases are equal, as are all $\Delta\mu_i$, and finally also the chemical potential μ_1 of the reference compound. Now consider what happens if we supersaturate the parent phase, for instance by compression (the analysis for the case of supercooling follows by analogy). In the semigrand ensemble we perform this supersaturation by increasing P, while keeping T and all $\Delta\mu_i$ constant. Note that this route need not correspond to the physical route for supersaturation. The reason is the physical route is (usually) to supersaturate *at constant composition*. But in that case, all $\Delta\mu_i$ change by different amounts, and this is precisely the factor that complicates the analysis of nucleation in multicomponent systems.

Suppose that we have compressed the system up to a pressure P_β where μ_1 (and thereby all μ_i) in the parent phase have increased by an amount $\Delta\mu^\beta$. An equal compression of the phase α leads to an increase $\Delta\mu^\alpha$ in the chemical potential of all species in that phase. Obviously, $\Delta\mu^\alpha$ is less than $\Delta\mu^\beta$, because beyond coexistence, phase β is metastable. However, we can compress phase α to a higher pressure P_α such that

$$\Delta\mu^\alpha(P_\alpha) = \Delta\mu^\beta(P_\beta). \qquad \text{(C8)}$$

Note that, as we are working in the semigrand ensemble where we keep all $\Delta\mu_i$ constant, we have thus achieved equality of the chemical potentials in the two phases for *all* species in the multicomponent mixture. In homogeneous nucleation, it is the Laplace pressure Δp that ensures that the chemical potential of every individual species is equal inside and outside the critical nucleus. We can therefore make the immediate identification,

$$\Delta p = P_\alpha - P_\beta. \qquad \text{(C9)}$$

Of course, once we have determined the pressure P_α, then the density and composition of phase α follow.

In a simulation, we can solve equation (C8) by making use of the fact that, for a semigrand ensemble we have the following relation:

$$\frac{\partial\mu_1}{\partial P} = \frac{V}{N}. \qquad \text{(C10)}$$

We can compute the average volume V in a semigrand simulation, and hence we can obtain $\Delta\mu$ by integration. Our expression for the Laplace pressure then becomes

$$\int_{P_{\mathrm{coex}}}^{P_\beta + \Delta p} \langle V(P)\rangle_\alpha \, dP = \int_{P_{\mathrm{coex}}}^{P_\beta} \langle V(P)\rangle_\beta \, dP. \qquad \text{(C11)}$$

This can also be written as

$$\int_{P_\beta}^{P_\beta + \Delta p} \langle V(P)\rangle_\alpha \, dP = \Delta\mu^\beta(P_\beta), \qquad \text{(C12)}$$

For an incompressible system, we can simplify this expression further, but we will not do this here. Once we have computed Δp, we can estimate the interfacial free-energy γ_s by using our numerical information about the nucleation barrier ΔG, using Eq. (C7),

$$\gamma_s = \left(\frac{3}{16\pi}\right)^{1/3} \Delta G^{1/3}\Delta p^{2/3}.$$

[1] W. Hoover and F. Ree, J. Chem. Phys. **49**, 3609 (1968).
[2] A. Vrij *et al.*, Faraday Discuss. Chem. Soc. **76**, 19 (1983).
[3] P. Pusey and W. van Megen, Nature (London) **320**, 340 (1986).
[4] A. van Blaaderen and P. Wiltzuis, Science **270**, 1177 (1995).
[5] M. Rutgers, J. Dunsmuir, J. Xue, W. Russel, and P. Chaikin, Phys. Rev. B **53**, 5043 (1995).
[6] K. Schätzel and B. Ackerson, Phys. Rev. E **48**, 3766 (1993).
[7] J. Harland and W. van Megen, Phys. Rev. E **55**, 3054 (1997).
[8] C. Sinn, A. Heymann, A. Stipp, and T. Palberg, Prog. Colloid Polym. Sci. **118**, 266 (2001).
[9] S. Auer and D. Frenkel, Nature (London) **409**, 1020 (2001).
[10] W. van Megen, Transp. Theory Stat. Phys. **24**, 1017 (1995).
[11] A. Heymann, C. Stipp, C. Sinn, and T. Palberg, J. Colloid Interface Sci. **206**, 119 (1998).
[12] T. Palberg, J. Phys.: Condens. Matter **11**, 323 (1999).
[13] R. Davidchack and B. Laird, Phys. Rev. Lett. **85**, 4751 (2000).
[14] H. Reiss and R. Bowles, J. Chem. Phys. **111**, 7501 (1999).
[15] P. R. ten Wolde, Ph.D. thesis, University of Amsterdam, Amsterdam, The Netherlands, 1998.
[16] P. L. Steinhardt, D. R. Nelson, and M. Ronchetti, Phys. Rev. B **28**, 784 (1983).
[17] J. S. van Duijneveldt and D. Frenkel, J. Chem. Phys. **96**, 4655 (1992).
[18] P. R. ten Wolde, M. Ruiz-Montero, and D. Frenkel, Phys. Rev. Lett. **75**, 2714 (1995).
[19] P. R. ten Wolde, M. Ruiz-Montero, and D. Frenkel, Faraday Discuss. **114**, 9932 (1996).
[20] G. Torrie and J. Valleau, Chem. Phys. Lett. **28**, 578 (1974).
[21] D. Frenkel and B. Smit, *Understanding Molecular Simulations: From Algorithms to Applications* (Academic, San Diego, 1996).
[22] C. Geyer and E. Thompson, J. Am. Stat. Assoc. **90**, 909 (1995).
[23] W. Press, S. Teukolsky, W. Vetterling, and B. Flannery, *Numerical Recipies* (Cambridge University Press, Cambridge, 1992).
[24] A. Cacciuto, S. Auer, and D. Frenkel, J. Chem. Phys. **119**, 7467 (2003).
[25] S. Auer and D. Frenkel, Nature (London) **413**, 711 (2001).
[26] D. Chandler, J. Chem. Phys. **68**, 2959 (1978).
[27] M. Ruiz-Montero, D. Frenkel, and J. Brey, Mol. Phys. **90**, 925 (1997).
[28] P. R. ten Wolde, M. Ruiz-Montero, and D. Frenkel, J. Chem. Phys. **110**, 1591 (1999).
[29] B. Cichocki and K. Hinson, Physica A **166**, 473 (1990).
[30] M. Medina-Noyola, Phys. Rev. Lett. **60**, 2705 (1988).
[31] J. S. van Duijneveldt and H. N. W. Lekkerkerker, in *Science and Technology of Crystal Growth*, edited by J. P. van der Ecrden and O. S. L. Bruinsma (Kluwer-Academic, Dordrecht, 1995).
[32] Z. Cheng, Ph.D. thesis, Princeton University, Princeton, 1998.
[33] W. van Megen and S. M. Underwood, Phys. Rev. E **49**, 4206 (1994).
[34] W. Ostwald, Z. Phys. Chem., Stoechiom. Verwandtschaftsl. **22**, 289 (1897).
[35] S. Alexander and J. McTague, Phys. Rev. Lett. **41**, 702 (1978).
[36] W. Klein and F. Leyvraz, Phys. Rev. Lett. **57**, 2845 (1986).
[37] W. Klein, Phys. Rev. E **64**, 056110 (2001).
[38] S. Pronk and D. Frenkel, J. Chem. Phys. **110**, 4589 (1999).
[39] S. Mau and D. Huse, Phys. Rev. E **59**, 4396 (1999).
[40] P. Pusey *et al.*, Phys. Rev. Lett. **63**, 2753 (1989).
[41] M. Elliot, S. Haddon, and W. Poon, J. Phys.: Condens. Matter **13**, 553 (2001).
[42] J. Zhu *et al.*, Nature (London) **387**, 883 (1997).
[43] P. Bolhuis, D. Chandler, C. Dellago, and P. Geissler, Annu. Rev. Phys. Chem. **53**, 291 (2002).
[44] J. M. Polson, E. Trizac, S. Pronk, and D. Frenkel, J. Chem. Phys. **112**, 5339 (2000).
[45] K. Hall, J. Chem. Phys. **57**, 2252 (1970).